Scale-bridging analysis of heterogeneous deformation behavior in austenitic stainless steel

Koki Yamamoto[a], Toshio Ogawa[*a], Zhilei Wang[a], and Yoshitaka Adachi[a]

[a]Department of Materials Design Innovation Engineering, Graduate School of Engineering, Nagoya University, Furo-cho, Chikusa-ku, Nagoya, Aichi 464-8603, Japan

*Corresponding author.

Department of Materials Design Innovation Engineering, Graduate School of Engineering, Nagoya University, Furo-cho, Chikusa-ku, Nagoya, Aichi 464-8603, Japan

E-mail address: ogawa.toshio@material.nagoya-u.ac.jp (Toshio Ogawa)

Tel: +81-52-789-3579

Fax: +81-52-789-4858

Abstract

In this study, scale-bridging analysis of heterogeneous deformation behavior in SUS310S austenitic stainless steel was conducted using X-ray line profile analysis, digital image correlation (DIC), and transmission electron microscopy (TEM). Specimens were prepared using tensile strain of 3%–40% at 298 ± 2 K. According to the X-ray line profile analysis, increasing strain increased dislocation density and decreased crystallite size. Furthermore, using DIC, low- and high-strain regions were observed in the early stages of deformation. TEM analysis showed that dislocations in the low-strain region were rarely tangled, while in the high-strain region, tangled dislocation and increased dislocation density were observed. TEM analysis also demonstrated that the formation of dislocation cells was promoted in the later stages of deformation, and the size of dislocation cells decreased as the strain increased. Moreover, we showed quantitative relationships between dislocation density, dislocation cell size, and crystallite size based on our findings.

Keywords: austenitic stainless steel; dislocation substructure; heterogeneous deformation; scale-bridging analysis

1. Introduction

Stainless steel is widely used in various industrial fields because of its excellent mechanical properties. To improve the safety and reliability of stainless steel, a thorough analysis of the deformation behavior is required. Deformation behavior was recently investigated using digital image correlation (DIC) method [1–3]. DIC is a cutting-edge, noncontact, optical technique for determining metal strain and displacement. Tabata *et al.* [1] used the DIC method to examine the plastic deformation behavior of single phase ferrite steel and suggested that it can be used to evaluate heterogeneous strain distributions.

In addition to the macroscale analysis of heterogeneous deformation behavior, microscale analysis is required to precisely control the mechanical properties of stainless steel. Transmission electron microscopy (TEM) has long been used to observe low-angle grain boundaries and dislocation cell structures with local misorientation. TEM is used to obtain the Kikuchi patterns in a local area, such as the region within a dislocation cell.

The macro and microscale analyses of heterogeneous deformation behavior were performed separately; nevertheless, they should be accomplished systematically. The number of studies on scale-bridging analysis of heterogeneous deformation behavior is limited. X-ray line profile analysis employing modified Williamson–Hall and Warren–Averbach methods has been used in the quantitative analysis of dislocation substructure [4–6]. These methods indicate average information of the dislocation substructure, such as dislocation density and crystallite size [7,8]. In addition to the DIC and TEM analyses, the scale-bridging analysis of heterogeneous deformation behavior can be achieved using the modified Williamson–Hall and Warren–Averbach methods. This research aims to use X-ray line profile analysis, DIC, and TEM to perform scale-bridging analysis of heterogeneous deformation behavior in SUS310S austenitic stainless steel. In particular, we focused on showing quantitative relationships between dislocation density, dislocation cell size, and crystallite size.

2. Experimental procedures

SUS310S austenitic stainless-steel sheet with a thickness of 1.0 mm was used in the experiments. After the annealing at 1273 K for 15 min, specimens were prepared by applying tensile strain of 3%–40% at 298 ± 2 K.

X-ray line profile analysis was used to evaluate the dislocation density and crystallite size. An X-ray diffractometer (RINT2500, Rigaku, Tokyo, Japan), with Mo Kα radiation of λ = 0.071073 nm at 50 kV and 200 mA was used to obtain X-ray diffraction patterns of the specimens.

The microstructures in the rolling direction–transverse direction (RD–TD) plane of the specimens were examined using a scanning electron microscope (SEM; JSM-7001FA, JEOL, Tokyo, Japan). Additionally, the strain distributions in the RD–TD plane at the same area as the SEM observation were evaluated using DIC (VIC-2D, Correlated Solutions Inc., SC, USA) with a subset size of 43 × 43 pixels and a step of 5 × 5 pixels.

The specimens for cross-sectional TEM analysis were prepared using ion thinning method. Additionally, a focused ion beam (FIB)-SEM instrument (Ethos NX5000, Hitachi, Tokyo, Japan) was used for TEM specimen preparation to examine the local region of microstructure. Dislocation substructures were observed using TEM (JEM-2100 plus, JEOL, Tokyo, Japan) operated at 200 kV. The dislocation cell size was measured using linear intercept method (ASTM E112).

3. Results and discussion

Figure 1 demonstrates the effect of strain on the dislocation density and crystallite size during deformation. By increasing strain, the dislocation density increased (Figure 1a), while

the crystallite size decreased (Figure 1b). Hereafter, the average information of dislocation substructure and data obtained through other methods of analysis is comprehensively discussed. Figure 2 displays the SEM images and DIC strain maps in a specimen with 6% strain, in which low-strain regions can be observed. To observe the dislocation substructures in the low- and high-strain regions, TEM specimens were prepared using FIB. Figure 2b and 2c show the typical dislocation substructures of the specimen with 6% strain in the low- and high-strain regions, respectively. Although dislocations were observed in the low-strain region, they were rarely tangled (Figure 2b). Thus, the existence of low-strain regions indicates the presence of regions with slightly modified dislocation substructure. This finding contradicts the one shown in Figure 1. In the high-strain region, however, tangled dislocation and increased dislocation density were confirmed (Figure 2c), consistent with that shown in Figure 1. Because the results shown in Figure 1 are the average information of dislocation substructure, these results indicate that deformation analysis should be performed at different scales. Figure 3 displays typical dislocation substructures for specimens with 20% and 40% strain. The specimen with 6% strain (Figures 2b and 2c) had rarely seen pronounced dislocation cells, while these cells were clearly visible in specimens with 20% and 40% strain (Figures 3a and 3b). The dislocation density increases with increasing strain (Figure 1a), and this result agrees with that obtained through TEM observation.

The average size of dislocation cells in specimens with 20% and 40% strain was 0.417 and 0.354 μm, respectively. Notably, the dislocation cell walls in the specimen with 40% strain were more visible than those in the specimen with 20% strain. These findings suggest that as the strain increases, the size of dislocation cells decreases and the visibility of the dislocation cell walls increases. The relationship between the size of dislocation cells and dislocation density has been previously reported [9]. The size of dislocation cells is expressed as

$$d = k\rho^{-\frac{1}{2}} \tag{1}$$

where d is the size of dislocation cells, k is a constant, and ρ is the dislocation density. According to Eq. (1), the size of dislocation cells decreases by increasing the dislocation density. Thus, the observed decrease in the size of dislocation cells with increasing strain (Figure 1a) in this study can be explained by Eq. (1). Moreover, the value of k can be estimated by substituting the experimentally obtained values of d and ρ into Eq. (1). As a result, regardless of the strain, the value of k was estimated to be ~14. As shown in Figure 1b, the crystallite size also decreased with increasing strain, suggesting that the dislocation cell size and crystallite size are correlated. Regardless of strain, the dislocation cell size was ~29 times that of the crystallite size. The correlation between the cold reduction rate and crystallite size was difficult to confirm because the change in the crystallite size by increasing the cold reduction rate was very small [10]. The change in the crystallite size by increasing strain is certainly small; however, the result shown in Figure 1b indicates that the slight change in the crystallite size by increasing strain was successfully detected. As mentioned above, the dislocation density, dislocation cell size, and crystallite size are correlated and can be expressed as follows

$$d = 14\rho^{-\frac{1}{2}} = 29D \tag{2}$$

where D is the average crystallite size.

4. Conclusions

X-ray line profile analysis, DIC, and TEM were used in this study to conduct a scale-bridging analysis of heterogeneous deformation behavior in SUS310S austenitic stainless steel. Low- and high-strain regions were observed in the strained specimen during the early stage of deformation. TEM observation revealed that dislocations were rarely tangled in the low-strain region, while the high-strain region showed tangled dislocation and increased dislocation density. Because these results are not necessarily in agreement with the X-ray line profile

analysis results, the analysis of heterogeneous deformation should be performed at different scales. In the later stage of deformation, the formation of dislocation cells was promoted, and the dislocation cell size decreased by increasing strain. Results obtained through TEM are in agreement with the X-ray line profile analysis results, thus implying that the average information of dislocation substructure tends to reflect the local dislocation substructure when the strain amount is large.

References

[1] R. Tabata, H. Tsuruzono, S. Sadamatsu, Y. Adachi, Digital image correlation analysis of plastic deformation behavior of ferrite in Fe-Mn-Si alloy, J. Jpn. Soc. Heat Treat. 55 (2015) 368–377.

[2] D. Yan, C. C. Tasan, D. Raabe, High resolution in situ mapping of microstrain and microstructure evolution reveals damage resistance criteria in dual phase steels, Acta Mater. 96 (2015) 399–409.

[3] M. Kamaya, M. Kawakubo, A procedure for determining the true stress–strain curve over a large range of strains using digital image correlation and finite element analysis, Mech. Mater. 43 (2011) 243–253.

[4] B. E. Warren, B. L. Averbach, The effect of cold-work distortion on X-ray patterns, J. Appl. Phys. 21 (1950) 595–599.

[5] T. Ungár, A. Borbély, The effect of dislocation contrast on x-ray line broadening: A new approach to line profile analysis, Appl. Phys. Lett. 69 (1996) 3173–3175.

[6] T. Ungár, S. Ott, P. G. Sanders, A. Borbély, J. R. Weertman, Dislocations, grain size and planar faults in nanostructured copper determined by high resolution X-ray diffraction and a new procedure of peak profile analysis, Acta Mater. 46 (1998) 3693–3699

[7] D. Akama, T. Tsuchiyama, S. Takaki, Change in dislocation characteristics with cold working in ultralow-carbon martensitic steel, ISIJ Int. 56 (2016) 1675–1680.

[8] T. Shintani, Y. Murata, Evaluation of the dislocation density and dislocation character in cold rolled Type 304 steel determined by profile analysis of X-ray diffraction, Acta Mater. 59 (2011) 4314–4322.

[9] S. V. Raj, G. M. Pharr, A compilation and analysis of data for the stress dependence of the subgrain size, Mater. Sci. Eng. 81 (1986) 217–237.

[10] S. Takaki, T. Masumura, F. Jiang, T. Tsuchiyama, Evaluation of dislocation density in cold

worked low carbon ferritic steel, Tetsu-to-Hagané 104 (2018) 683–688.

Figure captions

Figure 1 Changes in (a) dislocation density and (b) crystallite size as a function of strain.

Figure 2 (a) SEM images and DIC strain maps of a specimen with 6% strain. Typical dislocation substructures of (b) low- and (c) high-strain regions in (a).

Figure 3 Typical dislocation substructures of specimens with (a) 20% and (b) 40% strain.

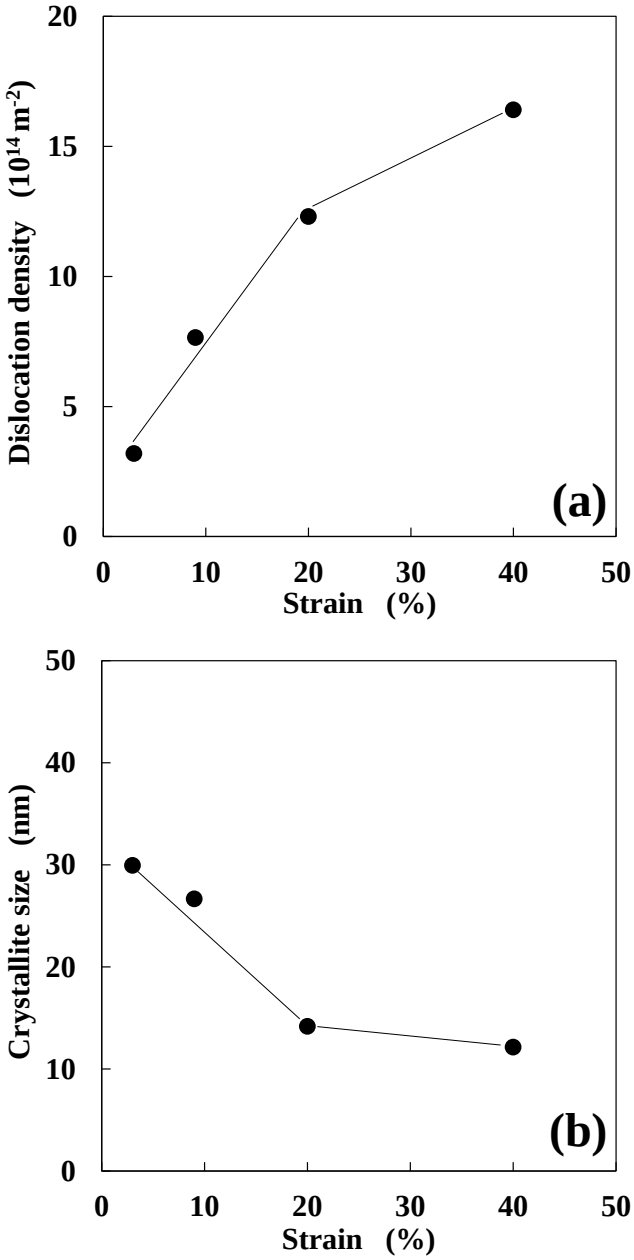

Figure 1 Changes in (a) dislocation density and (b) crystallite size as a function of strain.

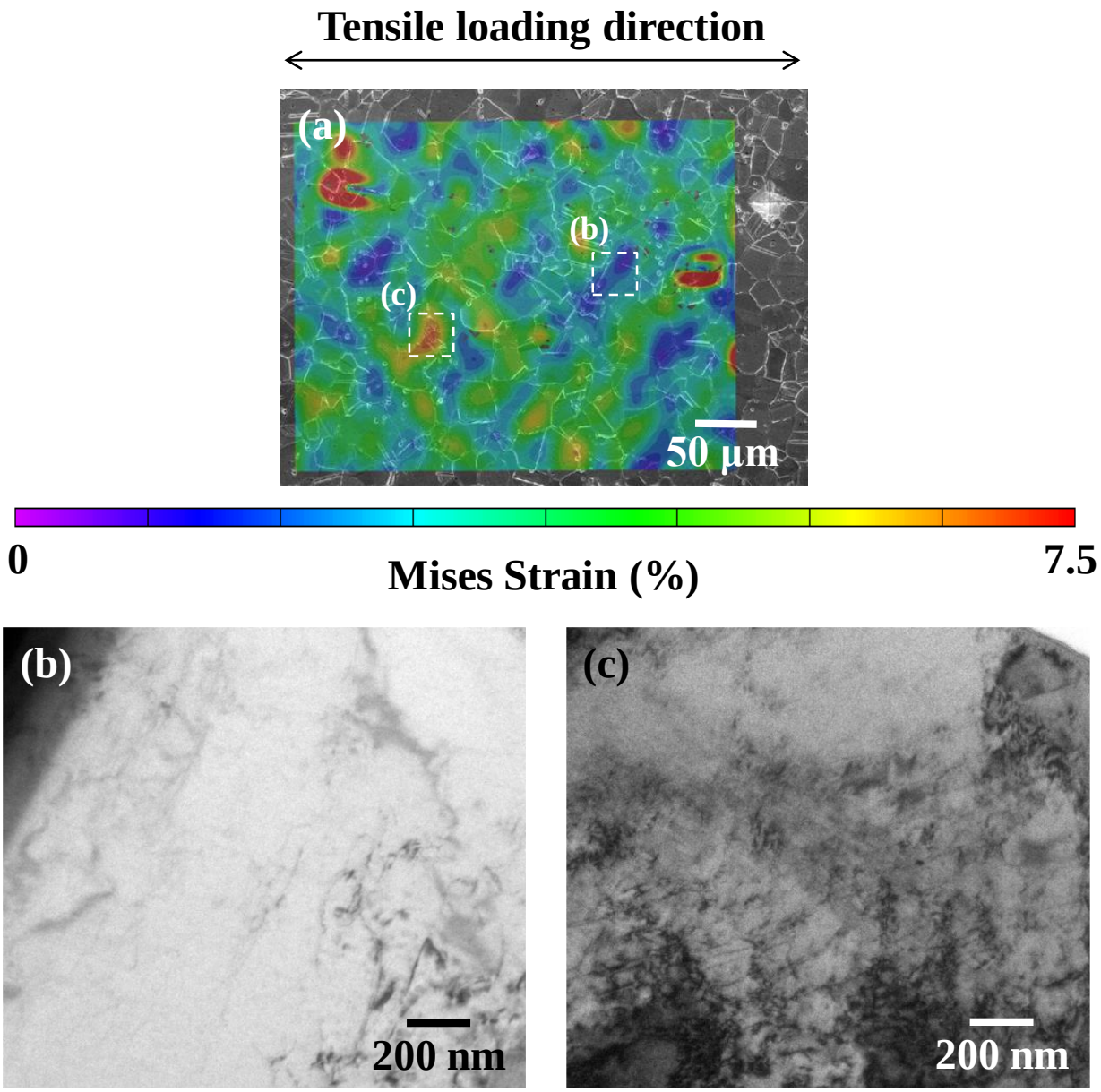

Figure 2 (a) SEM images and DIC strain maps of a specimen with 6% strain. Typical dislocation substructures of (b) low- and (c) high-strain regions in (a).

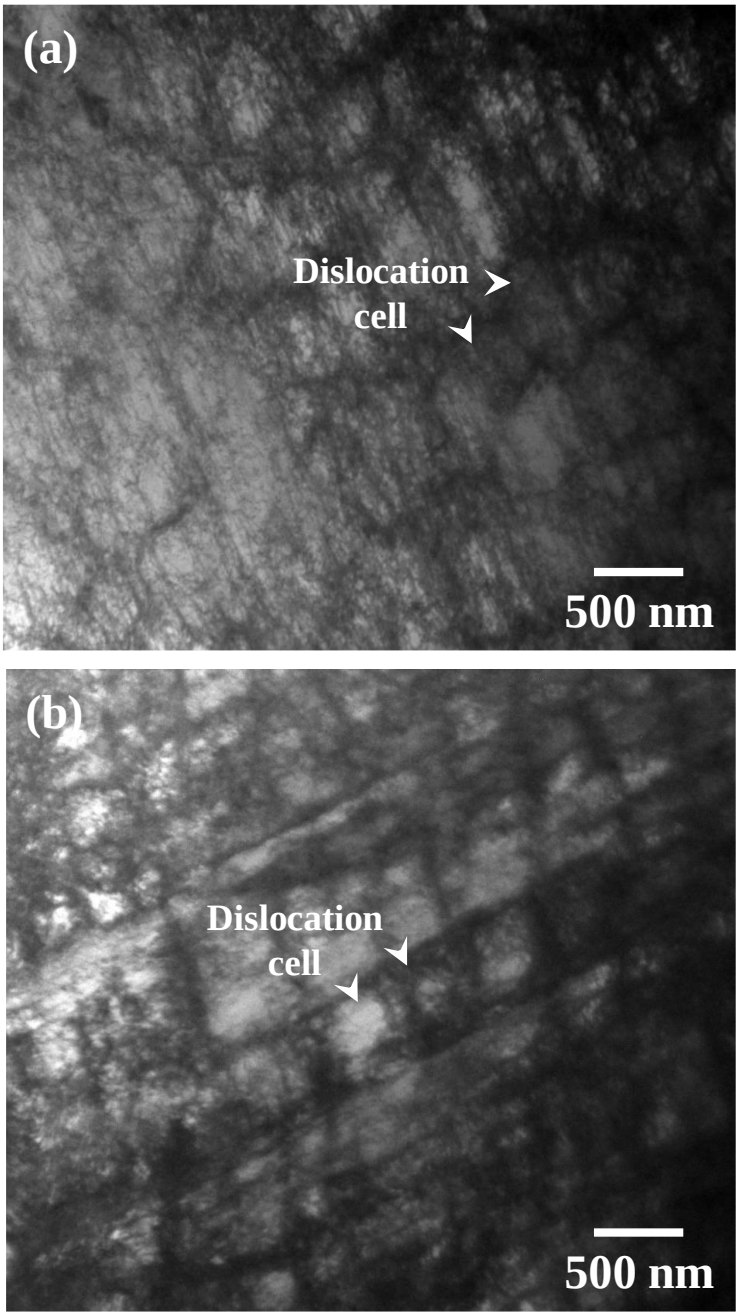

Figure 3 Typical dislocation substructures of specimens with (a) 20% and (b) 40% strain.